Evolution of Ocean circulation in the North Atlantic Ocean during the Miocene: impact of the Greenland ice sheet and the Eastern Tethys Seaway

Q. Pillot, Y. Donnadieu, A.-C. Sarr, J.-B. Ladant, B. Suchéras-Marx

Paleoceanography and Paleoclimatology

AGU ADVANCING EARTH AND SPACE SCIENCE

RESEARCH ARTICLE
10.1029/2022PA004415

Key Points:

- Ocean circulation induced by Early Miocene paleogeography in the IPSL-CM5A2 Earth System model is studied
- No clear impact of the closure of the Eastern Tethys Seaway is found
- Significant increase in North Atlantic Deep Water intensity results from ephemeral Greenland ice-sheets during the Miocene

Supporting Information:

Supporting Information may be found in the online version of this article.

Correspondence to:

Q. Pillot,
pillot@cerege.fr

Citation:

Pillot, Q., Donnadieu, Y., Sarr, A.-C., Ladant, J.-B., & Suchéras-Marx, B. (2022). Evolution of ocean circulation in the North Atlantic Ocean during the Miocene: Impact of the Greenland Ice Sheet and the Eastern Tethys Seaway. *Paleoceanography and Paleoclimatology*, *37*, e2022PA004415. https://doi.org/10.1029/2022PA004415

Received 13 JAN 2022
Accepted 9 AUG 2022

Author Contributions:

Conceptualization: Y. Donnadieu
Data curation: Q. Pillot
Formal analysis: Q. Pillot
Funding acquisition: Y. Donnadieu, B. Suchéras-Marx
Investigation: Q. Pillot, Y. Donnadieu, A.-C. Sarr, J.-B. Ladant
Methodology: Y. Donnadieu, A.-C. Sarr
Project Administration: Y. Donnadieu
Software: Q. Pillot
Supervision: Y. Donnadieu, B. Suchéras-Marx
Validation: Q. Pillot, Y. Donnadieu, A.-C. Sarr
Writing – original draft: Q. Pillot, Y. Donnadieu, A.-C. Sarr, J.-B. Ladant, B. Suchéras-Marx
Writing – review & editing: Q. Pillot, Y. Donnadieu, A.-C. Sarr, J.-B. Ladant, B. Suchéras-Marx

Evolution of Ocean Circulation in the North Atlantic Ocean During the Miocene: Impact of the Greenland Ice Sheet and the Eastern Tethys Seaway

Q. Pillot[1], Y. Donnadieu[1], A.-C. Sarr[1], J.-B. Ladant[2], and B. Suchéras-Marx[1]

[1]CEREGE, Aix Marseille University, CNRS, IRD, INRAE, Coll. France, Aix-en-Provence, France, [2]Laboratoire des Sciences du Climat et de l'Environnement, LSCE/IPSL, CEA-CNRS-UVSQ, Université Paris-Saclay, Paris, France

Abstract The Modern Ocean is characterized by the formation of deep-water in the North Atlantic Ocean (i.e., NADW). This feature has been attributed to the modern geography, in which the Atlantic Ocean is a large basin extending from northern polar latitudes to the Southern Ocean, the latter enabling the connection of the otherwise isolated Atlantic with the Pacific and Indian Oceans. Sedimentary data date the establishment of the NADW between the beginning of the Eocene (~49 Ma) and the beginning of the Miocene (~23 Ma). The objective of this study is to quantify the impact of Miocene geography (~20 Ma) on NADW using new simulations performed with the Earth System Model IPSL-CM5A2. We specifically focus on the closure of the Eastern Tethys Seaway (ETS), dated between 22 and 14 Ma, which allowed the connection between the Atlantic and Indian Oceans, and on the Greenland Ice Sheet, whose earliest onset remains open to discussion but for which evidence suggest a possible existence as early as the Eocene. Our results show that the closure of the ETS does not appear to impact the establishment of NADW, because waters from the Indian Ocean do not reach the NADW formation zone when the seaway is open. Conversely, the existence of an ice sheet over Greenland strengthens the formation of NADW owing to topography induced changes in wind patterns over the North Atlantic, which in turn, results in a salinification of the North Atlantic and Nordic Seas, and in an increase in deep-water formation.

1. Introduction

The Atlantic Meridional Overturning Circulation (AMOC) is today the central feature of the Global ocean circulation (Talley, 2013). It is dominated by two overturning cells usually referred to as the Antarctic Bottom Water (AABW) and the North Atlantic Deep Water (NADW). The NADW forms mainly in the Norwegian Sea by winter open-ocean cooling of salt-rich water advected northward by the Gulf Stream. The cooling increases the density of surface waters, which results in vertical convection and the formation of deep water. The newly formed deep and dense waters flow southward to the Southern Ocean, where they are upwelled under the action of the Antarctic Circumpolar Current (ACC). They are then dragged either into the AABW overturning branch and redistributed in the Pacific and Indian basins via the ACC or into the formation area of the Antarctic Intermediate Water (AAIW), thereby flowing northward as (sub)surface currents and closing the AMOC cell (Talley, 2013). The structure of the modern AMOC results from the particular configuration of the Atlantic basin geometry with a closed Central American Seaway and an open Drake Passage (Ferreira et al., 2018). During Cenozoic times (66-0 Ma) and, in particular, the Miocene period (23-5 Ma), the physical structure of the AMOC was probably different compared to the present-day because the configuration of major gateways and submarine topographic barriers in the Atlantic and Pacific basins differ substantially (Hutchinson et al., 2019). From the early Miocene (~23 Ma) to today, these changes include the deepening of the Greenland-Scotland Ridge (Stärz et al., 2017), the opening of Fram Strait (Ehlers & Jokat, 2013) and Bering Strait (Gladenkov & Gladenkov, 2004) in the northern high latitudes; the closure of Central American Seaway (Montes et al., 2015) and Eastern Tethys Seaway (ETS, Bialik et al., 2019) in the tropics; and the potential narrowing of Drake Passage (Lagabrielle et al., 2009) in the southern high latitudes. Apart from those change in the seaways and the Eurasiatic landsea mask, the continental configuration during the Miocene period was close to the modern one with however some substantial changes in the topography worldwide such as lower elevation in major mountain belts (Andes, Himalayas, East Africa, and European ranges); see Poblete et al. (2021) for review.

Several studies investigated the geological history of deep water formation in the North Atlantic Ocean over the Cenozoic, both using Earth system models of various complexities and paleoceanographic data. Among those data, researchers have relied on sedimentary drift deposits, on Nd isotopes and on oxygen and carbon isotopes. Many of those studies suggest the onset of NADW formation during the Eocene (Borrelli et al., 2014; Coxall et al., 2018; Davies et al., 2001; Langton et al., 2016; Via & Thomas, 2006; Wright & Miller, 1993); the described water masses in such studies is sometimes called North Component Water (NCW) which refers to an early version of the NADW. The NCW was not part of a large and extensive overturning cell as the modern NADW. Borrelli et al. (2014) reported similar benthic foraminifera $\delta^{18}O$ and $\delta^{13}C$ signatures at site ODP1053 (upper deep water, western North Atlantic) and at sites located in the Southern Ocean, equatorial Pacific, and western Atlantic until the end of the middle Eocene (39-40 Ma). Around 38.5 Ma, the values between the North Atlantic Ocean, the Southern Ocean and the Pacific Ocean began to differentiate leading Borrelli et al. (2014) to suggest an onset of NCW due to a gradual opening of the Southern Ocean gateways. Langton et al. (2016) used the same methodology on sites further south in the Atlantic Ocean (30°S) and find a similar date for the initiation of NCW (38 Ma). Other studies rather propose that tectonic adjustments of the Greenland-Scotland Ridge initiated the NCW between 36 Ma (Coxall et al., 2018) and 34-33 Ma (Via & Thomas, 2006; Wright & Miller, 1993), as the Greenland-Scotland Ridge was likely too shallow at 38 Ma to enable the southward inflow of possible deep waters formed northward of the ridge in the Greenland and Norwegian Seas. Independent evidence from sedimentary deposits in the Faroe Shetland Basin indicate that NCW may have begun around 35 Ma (Davies et al., 2001). Later, the transition from NCW to NADW may have been initiated by the intensification of the ACC at a time of a deepening of the Drake Passage in the late Oligocene (Katz et al., 2011). Moreover, Scher and Martin (2008) correlated the widening of the Drake Passage with the intensification of NCW/NADW because the long-term decreasing trend in neodymium isotopes values on the Agulhas Ridge (Atlantic sector of the Southern Ocean) suggests that the export of NCW/NADW from the North Atlantic Ocean to the Southern Ocean increased during the Oligocene and Miocene. From Miocene onward, NADW dynamics has been influenced by other seaways. Cenozoic sediment cores from the Arctic deep seafloor revealed more ventilated waters in the Arctic Basin related to enhanced NADW about 17.5 Ma due to the opening of the Fram Strait and increased exchanges between North Atlantic Ocean and Artic basin (Jakobsson et al., 2007). Woodruff and Savin (1989) used isotopic data from benthic foraminifera to suggest that the closure of the ETS connecting the Indian Ocean to the Mediterranean Sea caused saltwater to enter the North Atlantic, intensifying NADW around 14.5 Ma. Short-term fluctuations in NADW after 12 Ma are controlled by vertical movements of the Greenland-Scotland Ridge (Poore et al., 2006) based on the study of $\delta^{13}C$ gradients in benthic foraminifera from several oceans (Atlantic, Pacific, and Southern Oceans).

From a modeling point of view, climate model studies operated with Eocene to Miocene paleogeographies have simulated meridional overturning circulation substantially different from the modern (Baatsen et al., 2020; Goldner et al., 2014; Hutchinson et al., 2018; Toumoulin et al., 2020; von der Heydt & Dijkstra, 2006). The details of deep-water formation zones and water mass pathways are generally specific to each study because both heavily depend on the model and paleogeography employed; better agreement between models is obtained when the same paleogeography is used (Lunt et al., 2021). Numerous work has explored in particular the sensitivity of the MOC and AMOC to marine gateways during the middle-late Cenozoic (Hutchinson et al., 2019; Stärz et al., 2017; Toumoulin et al., 2020; Z. Zhang et al., 2011) because major gateways (such as the Central American Seaway, the Drake Passage, the Eastern Tethys Seaway or the Greenland-Scotland Ridge) are known to substantially evolve across the last 40 Ma. With respect to the AMOC, modeling studies have long demonstrated that the closure of the Central American Seaway enabled an intensification of NADW formation (Nisancioglu et al., 2003; Schneider & Schmittner, 2006; Sepulchre et al., 2014). Coupled ocean/atmosphere simulations also indicate that the deepening of the Greenland-Scotland Ridge amplifies NADW intensity (Hossain et al., 2020; Stärz et al., 2017). In contrast, the opening of the Bering Strait decreases NADW intensity although this effect is offset by the closure of the Central American Seaway, according to other modeling studies (Brierley & Fedorov, 2016; Hu et al., 2015). Instead, the impact of the opening of Drake Passage on the AMOC is less consensual in model results (see discussion in Toumoulin et al. (2020)). Compared to other major seaways such as the Central American Seaway or Drake Passage, the ETS has only drawn limited attention (Hamon et al., 2013) and, to our knowledge, no recent study has tested the role of this seaway in the emergence and intensification of the NADW using up-to-date paleogeographies.

In the present study, we aim to discuss the dynamics of the NCW/NADW considering the complimentary angle of the closure of the ETS as well as of another potentially overlooked forcing of NCW/NADW changes during the Oligo-Miocene that is the Greenland Ice Sheet (GIS). In the following, we briefly review what is known about the Eocene to Miocene history of these two possible drivers of circulation changes. The tectonic history and closure chronology of the ETS is debated (Allen & Armstrong, 2008). Allen and Armstrong (2008) suggest a closure age during the late Eocene (~35 Ma), based on the study of deformation and uplift during the collision between the two tectonic plates. Hüsing et al. (2009) suggest a more recent age for the closure of the ETS (28 Ma, middle Oligocene) based on biostratigraphic studies in the north of the Bitlis-Zagros suture zone. However, many paleogeographic and paleontological studies indicate an early Miocene closure (Harzhauser et al., 2009; Reuter et al., 2009; Rögl, 1999). Bialik et al. (2019) use neodymium isotope records from both sides of the seaway and suggest that water mass exchange between the Mediterranean Sea and Indian Ocean was reduced by 90% around 20 Ma. This age is also proposed by Okay et al. (2010) using apatite fission track ages from the Bitlis-Zagros thrust zone. Biostratigraphical and paleontological data indicate that the Mediterranean Basin and Indian Ocean were intermittently connected until at least the middle Miocene (Harzhauser et al., 2007, 2009; Rögl, 1999; Sun et al., 2021). Through magnetostratigraphic and biostratigraphic studies on sediments from the Zagros Basin, Sun et al. (2021) indicate that the ETS evolved from partially open to fully closed across the early and middle Miocene. Most studies converge to date the final closure to the middle and late Miocene between 14 and 11 Ma (Bialik et al., 2019; Hüsing et al., 2009; Rögl, 1999; Sun et al., 2021). The temporal proximity with the Mid-Miocene climate Transition (e.g., Pierce et al., 2017) hints at a causal relationship between the significant drop in sea level driven by the growth of the ice sheet over Antarctica and the final closure of the ETS (Bialik et al., 2019; Sun et al., 2021). The history of Greenland glaciations is unclear. There is debated evidence of the existence of the ice sheet dating back to the Eocene (Eldrett et al., 2007; Tripati et al., 2008) in the form of Ice-Rafted Debris (IRD) in the Norwegian Sea. Thermochronological constraints argue for the presence of ice sheet-enhanced erosion during the early Oligocene (Bernard et al., 2016). Other work has documented glaciations during the late Miocene (11 and 7 Ma) through the presence of IRD and dropstones in Irminger Basin sediments (Bierman et al., 2016; Helland & Holmes, 1997; John & Krissek, 2002), yet the consensus is still that the perennial glaciation of Greenland occurred at the Plio-Pleistocene transition, based on sedimentological analyses from the East Greenland margin (Butt et al., 2001), marine seismic reflection (contourites) from the West Greenland margin (Knutz et al., 2015), as well as climate-ice sheet modeling (Lunt et al., 2008; Tan et al., 2018). Finally, using an isotope-capable global climate/ice-sheet model, DeConto et al. (2008) indicate that episodic glaciations in the Northern Hemisphere are possible since 25 Ma. Though still debated and not long-lasting, the GIS may have existed at times across the Oligo-Miocene but its impact on ocean circulation has never been tested in climate models of these geological stages, in contrast to modern configurations (Davini et al., 2015).

Here, we thus simulate the ocean dynamics using the IPSL-CM5A2 model with a fixed pCO_2 and updated paleogeography of the early Miocene proposed by Poblete et al. (2021), which exhibits open connections between the Pacific, Atlantic and Artic oceanic basins through the Central American Seaway, the Fram Strait, the Greenland-Scotland Ridge and the Drake Passage.

2. Methods

2.1. Model

The Earth System Model used in this study is IPSL-CM5A2 (Sepulchre et al., 2020) that is an updated version of IPSL-CM5A-LR model (Dufresne et al., 2013), with bias corrections and reduced computational times to perform multimillennial simulations typical of paleoclimate studies. It is composed of the NEMO ocean model (Madec & Team, 2015) which includes the PISCES-v2 model for biogeochemistry (Aumont et al., 2015), the OPA8.2 model for ocean dynamics (Madec & Team, 2015) and the LIM2 model for sea ice (Fichefet & Maqueda, 1997). IPSL-CM5A2 is also composed of the atmospheric model LMDZ (Hourdin et al., 2013) and the land surface and vegetation model ORCHIDEE (Krinner et al., 2005). The OASIS coupler (Valcke, 2013) connects the atmospheric grids (96×96 or 3.75° in longitude and 1.875° in latitude over 39 vertical levels) and oceanic grids (resolution of about 2° that decreases to 0.5° in the tropical region over 31 vertical levels, whose thickness varies from 10 m near the surface to 500 m near the bottom of the ocean). Model outputs have been averaged over the last 100 years of the simulation. More details about model parameterization can be found in Sepulchre et al. (2020). A simulation with pre-industrial conditions (modern geography, 280 ppm) was performed

Table 1
Experimental Design

Simulation	Geography	pCO_2	ETS	GIS	Simulation length
MioCTL	20 Ma	560 ppm	Closed	No	3,000 years
MioGIS	20 Ma	560 ppm	Closed	Yes	3,000 years
MioTet120	20 Ma	560 ppm	Open (120 m)	No	3,000 years
PREIND (Sepulchre et al., 2020)	Present-day	280 ppm	Closed	Yes	2,800 years

by Sepulchre et al. (2020) using the IPSL-CM5A2 model. This is the simulation we use here to compare Miocene climatic features with those from the preindustrial (noted PREIND hereafter, Table 1). In PREIND, the NADW reaches more than 2,000 m depth with a maximum flow of 11 Sv at 1,000 m depth and 45°N. The depth of the mixed layer exceeds 1,000 m south of Iceland and in the Greenland Sea. The AMOC is stronger and more consistent with observations in IPSL-CM5A2 than in IPSL-CM5A-LR, though the very active deep convection site south of Iceland remains inconsistent with observations.

2.2. Experiments and Boundary Conditions

Three simulations were run in this study with a paleogeography corresponding to the early Miocene (~20 Ma) from the study of Poblete et al. (2021) (Figure 1). In this paleogeography, most of the mountain belts are lower than today, there is a modern Antarctic ice-sheet and the Paratethys shallow sea covers part of Central and Eastern Europe with a connection to the Mediterranean Sea. The Central American Seaway is open but shallow, the Bering Strait is closed, the Fram Strait is narrower than today, and the Greenland-Scotland Ridge is deep (Figure 1). In absence of worldwide reconstruction for paleo-vegetation in the early Miocene, we used idealized vegetation with a latitudinal distribution. The atmospheric pCO_2 level for the three simulations is set to 560 ppm (Rae et al., 2021; Sosdian et al., 2018) and other parameters such as the other greenhouse gases and orbital parameters are set to their pre-industrial values. Simulations have been run for 3,000 years and reached quasi-equilibrium. Temperature trends computed over the last 500 years are 0.3 10^{-3}°C/yr for the surface and 0.2 10^{-3}°C/yr for the deepest layers of the ocean (Figure S2 in Supporting Information S1).

The first simulation (MioCTL, Table 1) is used as a reference for sensitivity tests. In this simulation there is no ice sheet on Greenland and the ETS is closed. This simulation was used in the Model intercomparison for the Miocene (Burls et al., 2021) and shows the same classical features as others models when compared to data with a good fit at low to mid-latitudes and a poorer fit to the global warmth inferred from data at higher latitudes. Simulating the low meridional temperature gradient reconstructed from Miocene data remains an outstanding problem for most models.

The second simulation, MioGIS, is identical to the first one but Greenland is covered by a modern-size ice sheet in order to maximize the potential of its direct effects on NADW—the elevation is larger and the albedo is higher compared to the no ice sheet case.

The third simulation, MioTet120, is identical to the control simulation, but the ETS is open with a depth of 120 m and a width of 390 km at its narrowest section. This depth was chosen to allow a significant surface flow exchange between the Mediterranean Sea and the Indian Ocean while agreeing with the configuration of a restricted pre-closure state.

3. Results and Discussion

3.1. Impacts of Miocene Paleogeography

Our MioCTL simulation exhibits spatial patterns of temperature and salinity relatively similar to the preindustrial simulation (PREIND, taken from Sepulchre et al. (2020)) with warm and salty waters extending northward across mid-latitudes in the eastern part of the northern North Atlantic basin (northern NA) while fresher and cooler waters spread over the western part covering the entire Labrador Sea (Figure 2a). Those water are brought toward the NA across the shallow early Miocene Fram Strait used in our paleogeography (Figure 1).

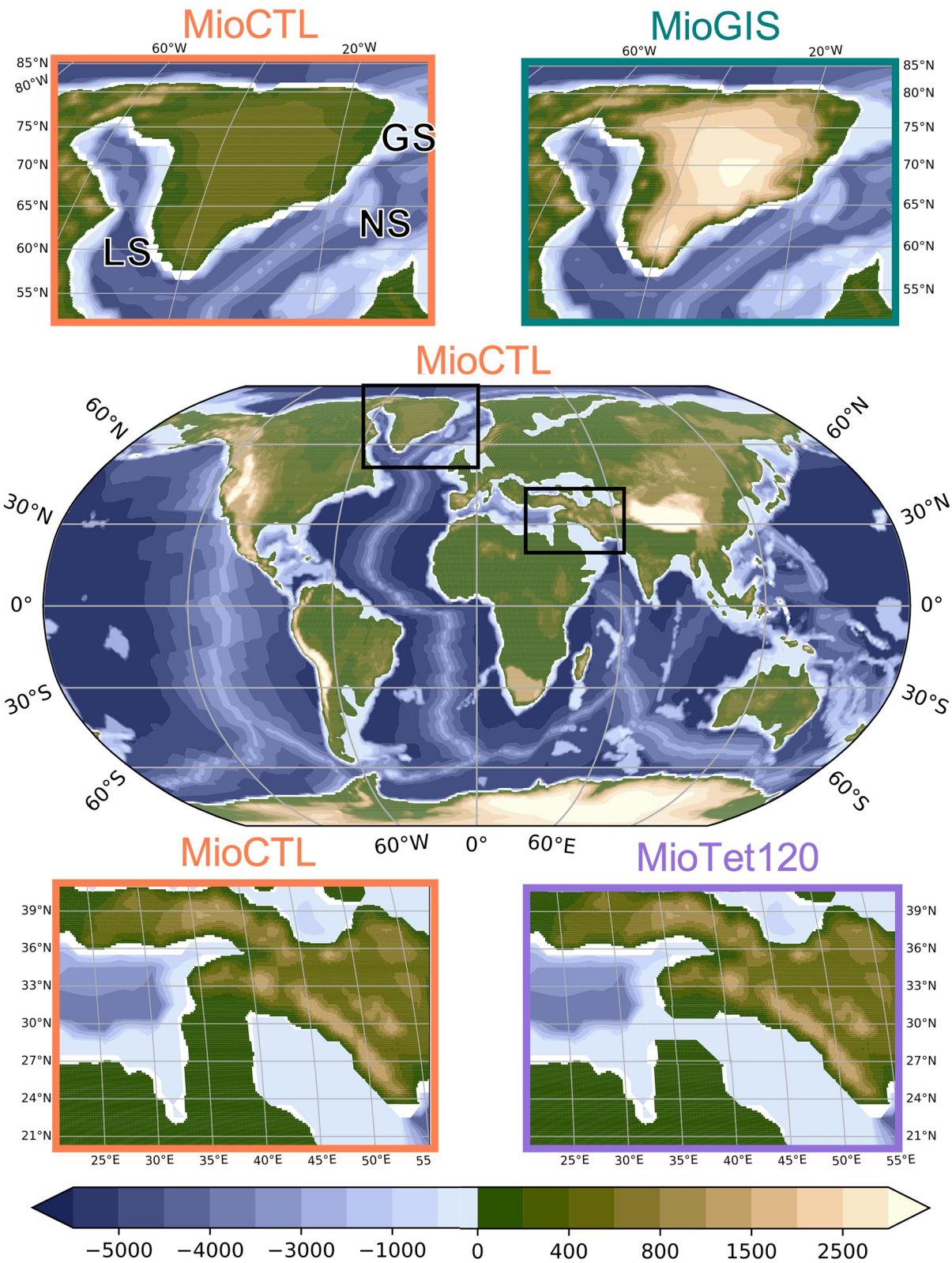

Figure 1. Topography and bathymetry of the simulations (in meters): MioCTL, MioGIS and MioTet120. A more detailed bathymetry is shown in Figure S1. LS: Labrador Sea. NS: Norwegian Sea. GS: Greenland Sea.

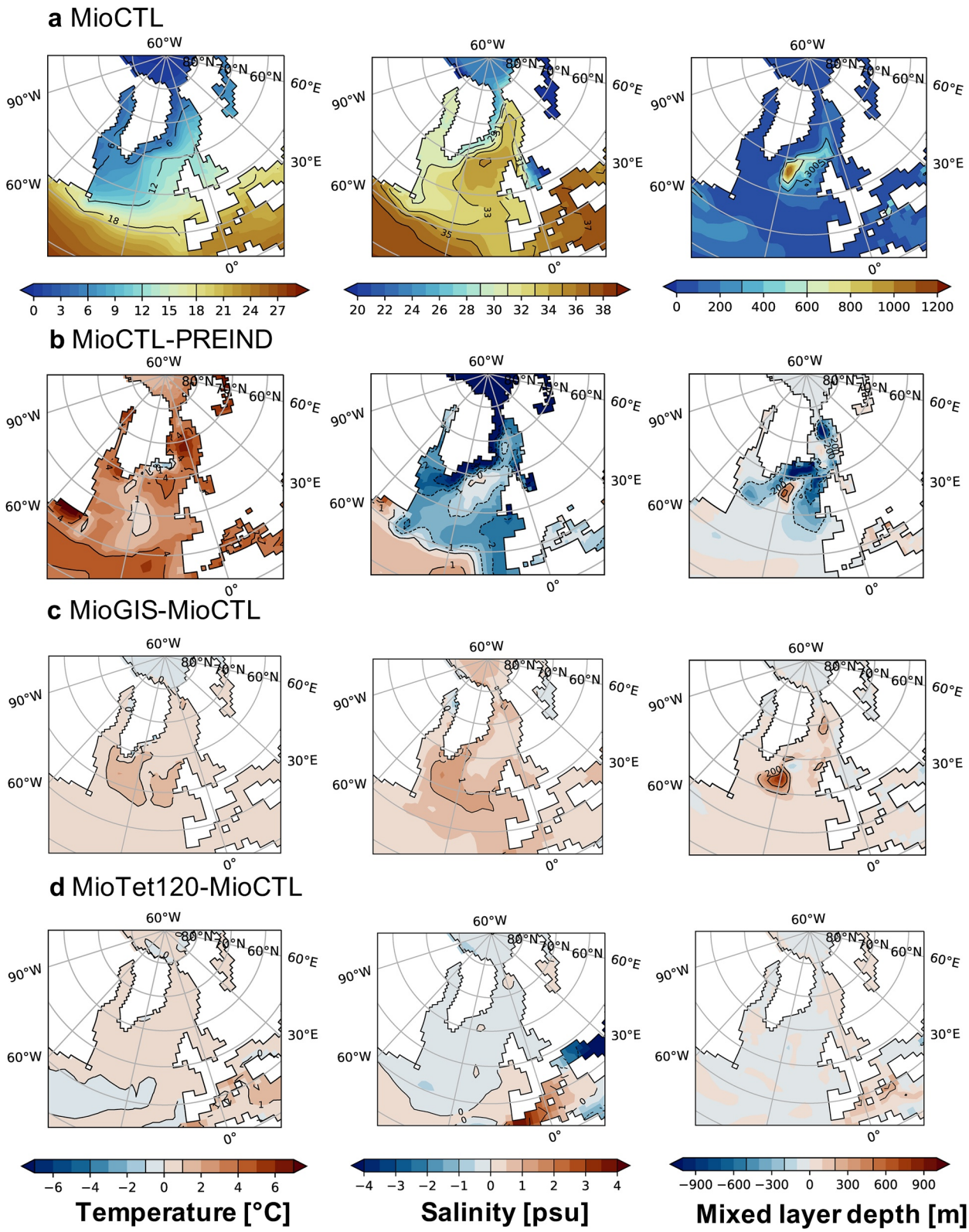

Figure 2. Left column, sea surface temperature (°C) averaged over the year. Middle column, sea surface salinity (psu) averaged over the year. Right column, mixed layer depth (mld, meter) averaged over the winter (January–February–March). (a) MioCTL simulation. (b) Difference between the MioCTL control simulation and the pre-industrial simulation (PREIND). (c) Difference between the MioGIS simulation and the MioCTL simulation. (d) Difference between the MioTet120 simulation and the MioCTL simulation. Values represent average on the last 100 years of each simulation.

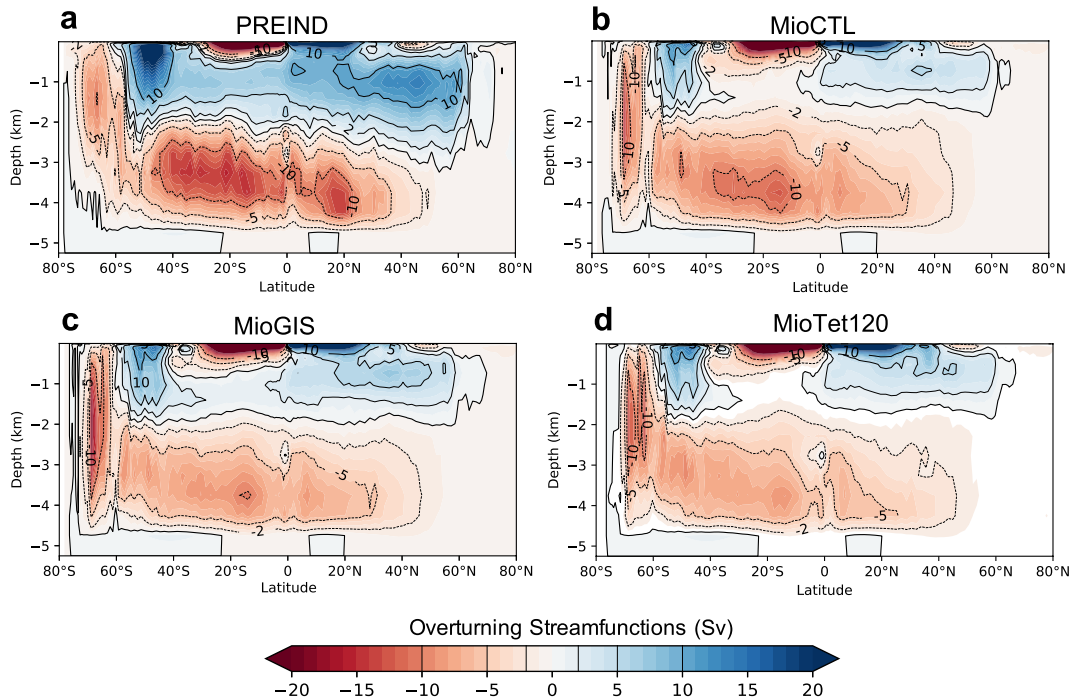

Figure 3. Global Meridional Overturning Circulation computed from the global ocean. (a) PREIND (b) MioCTL (c) MioGIS and (d) MioTet120. In blue, the water masses rotate clockwise and in red, counterclockwise. Unit: Sv; horizontal axis: latitude in degrees; vertical axis: depth in kilometers. Values represent average on the last 100 years of each simulation.

Deep water formation occurs in the North Atlantic Ocean over an area located between 20 and 30°W and between 55 and 60°N, as inferred by a deep winter mixed layer reaching locally 1,000 m. Comparison with modern features simulated in IPSL-CM5A2 (Figure 2) shows that the spatial extent of the sinking zone in the North Atlantic Ocean is reduced as well as the strength and vertical extension of the meridional overturning circulation (Figures 2b and 3). In the MioCTL simulation, the AMOC reaches 1,700 m in depth and extends to 60°S (Figure 3) with a maximum intensity of 5 Sv in the North Atlantic Ocean (at 37°N and 1,000 m) whereas the simulated preindustrial AMOC is 11 Sv and extends down to 3,000 m. This is in agreement with previous studies showing the major impact of the opened Central American Seaway on the intensity of NADW formation (Nisancioglu et al., 2003; Schneider & Schmittner, 2006; Sepulchre et al., 2014). We also note that our Miocene simulations were performed without tidal forcing in absence of an available reconstruction, which may induce a weaker overturning in the deepest layers of the ocean and explain the less intense AABW formation despite a deeper mixed layer depth found in our Miocene simulations (Y. Zhang et al., 2020). No deep water formation occurs in the North Pacific in any of our simulations. In the southern hemisphere, deep water areas are located both in the Atlantic and the Indian part of the Southern Ocean and mixed layer depth reach greater depth (1,000–2,500 m) than in the North Atlantic Ocean (Figure S3 in Supporting Information S1).

Because we have imposed a doubling of the atmospheric pCO_2, sea surface temperatures (SSTs) are warmer during the Miocene than at present-day with heterogeneous spatial patterns. This warming is particularly pronounced in two areas which are located first eastward of North America between 30 and 40°N and second in the Greenland-Iceland-Norwegian Seas with SST differences exceeding 5°C compared to PREIND (Figure 2b). Surface salinity is lower during the Miocene owing to the increased hydrological cycle occurring in a warmer climate at latitudes where the precipitation minus evaporation (P-E) budget is found to be positive (subtropics, Burls and Fedorov (2017); Herold et al. (2011)). In contrast, subtropical salinities are larger during the Miocene owing to a more negative P-E budget occurring at these latitudes (not shown). Finally, the positive salinity anomaly located southward of Greenland matches the only area where mixed layer depth is deeper in our MioCTL simulation compared to the PREIND simulation.

Herold et al. (2011) also observe a less intense NADW in their Miocene simulation compared to their modern simulation. In their Miocene simulation, the mixed layer depth (150 m) is much shallower than in MioCTL but

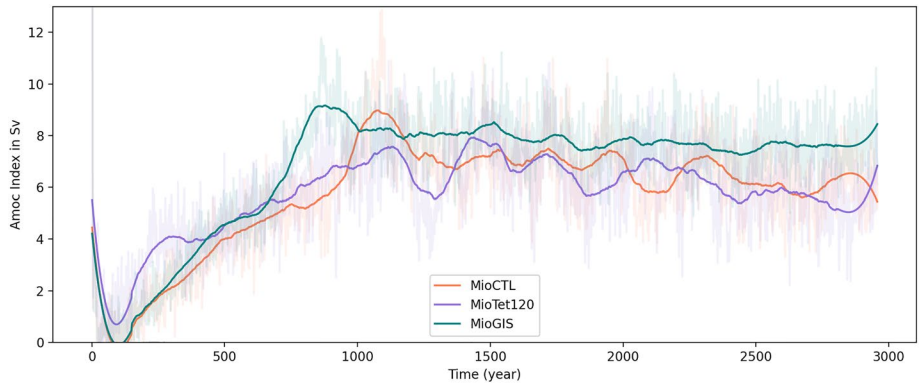

Figure 4. Temporal evolution of the AMOC index in Sv (yearly maximum of the meridional stream function between 38°N and 50°N and between 500 and 2,000 m depth) on the 3,000 years of simulations.

the NADW cell depth (1,500 m) is similar to MioCTL. The shallower deep water formation in the Miocene compared to the present day can be explained by less salty waters in the North Atlantic. However, they observe colder surface water temperatures in the Miocene than in the present. This is not in agreement with our results and is explained by the pCO_2 level in their simulations which is maintained at the same level in the Miocene as in their modern reference (355 ppm). Krapp and Jungclaus (2011) find no significant difference in the intensity of NADW and AMOC between their Miocene simulation and their modern simulation. This difference to our results can also be explained by their low pCO_2 level at 360 ppm because in another of their simulations with pCO_2 at 720 ppm, there is almost no NADW. This difference is also due to the salinity of surface waters in the North Atlantic Ocean which is equivalent in the Miocene and in the present (not the case in our study). They attribute this to the inflow of salt water from the Mediterranean Sea (open ETS) which compensates for the cooling by the Central American Seaway. The salinity input from the Mediterranean Sea when the ETS is open will be discussed below.

3.2. Ocean-Atmosphere Feedback Induced by the Greenland Ice-Sheet

With a GIS during the Miocene, the AMOC strengthens by 33% from 6 to 8 Sv (Figures 3 and 4) and the North Atlantic Ocean becomes saltier (0.5–1.5 psu increase). The formation zone of the NADW extends westward and covers the region 15° to 40°W and 50° to 60°N, and waters sink deeper down to 1,500 m (Figure 3c). An area of intermediate water formation also exists in the Greenland Sea (0°E, 70°N) in MioGIS, where the depth of the mixed layer reaches 500 m.

The presence of the ice-sheet topography in MioGIS compared to MioCTL modifies the spatial pattern of the low and high pressure cells over the Greenland, Labrador, Iceland and Nordic Seas (noted thereafter GLIN Seas, red contours on Figure 5). In the MioCTL simulation, there is an atmospheric low pressure cell east of Greenland that extends over land (Figure 6a). The center of this low pressure cell is located at latitude 67°N in the Norwegian Sea. The presence of the ice-sheet topography in MioGIS prevents this cell from advancing inland and its center is consequently further south than in MioCTL (57°N). Indeed, in MioGIS, a stable high-pressure area is present over Greenland, causing intense southwesterly winds along its southeastern coast (consistent with the results of Lunt et al. (2004) and Toniazzo et al. (2004)) and increasing the wind stress curl (Figures 6b and 6c). The surface divergence caused by these coastal winds and northeasterly winds (which constitute the south branch of the cyclonic circulation around the pressure low south of Greenland) favors mixing and vertical exchange through Ekman pumping. This increase in wind stress curl and vertical exchange with deeper, more saline waters induces a salinification of the GLIN seas. A positive salt-advection feedback is initiated (Ferreira et al., 2018) and brings more salt from the North Atlantic to the GLIN Seas in the MioGIS simulation. Indeed, the calculation of salt transport between the North Atlantic and GLIN Seas (Figure 5) shows that the presence of the GIS increases the exchange of salt by about 55%. In addition, the P-E budget over the GLIN Seas region is similar in both simulations but the runoff is slightly lower in MioGIS (−8 mSv, Figures 5 and S4 in Supporting Information S1). Overall, the GIS causes a lower freshwater input through changes in the hydrological cycle and a larger salt input controlled by changes in the wind forcing, both factors contributing to a larger mixing and a more intense AMOC.

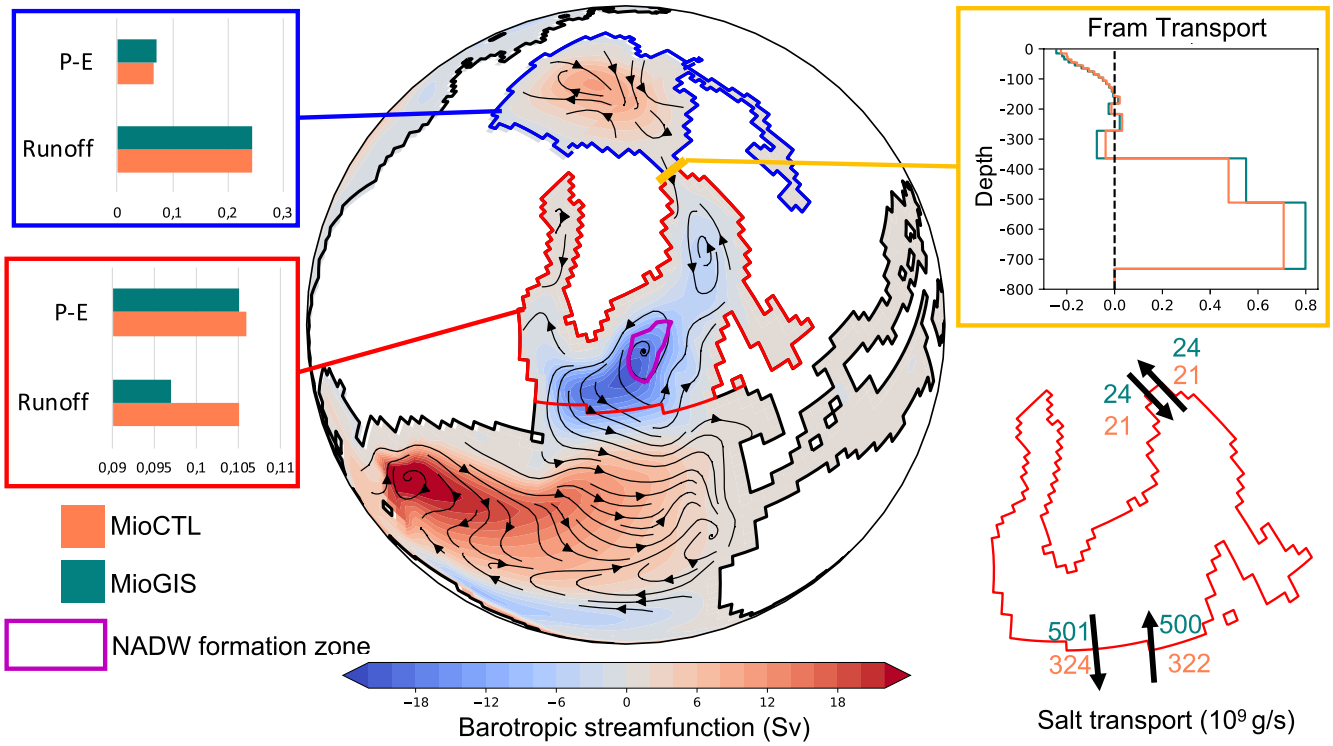

Figure 5. Mean annual barotropic stream function, in Sv, for the MioCTL simulation (in blue, the water masses rotate counterclockwise and in red, clockwise). The blue box shows the P-E balance and runoff (in Sv) for the Arctic basin. The red box shows the P-E balance and the runoff (in Sv) for the northern NA. The yellow box shows the water mass exchanges at the Fram Strait (in Sv), positive toward the north and negative toward the south. Bottom right, the salt transport budget (10^9 g/s). Values represent average on the last 100 years of each simulation.

More to the north, the GLIN Seas are connected to the Arctic across a much narrower Fram Strait. The presence of the GIS barely increases the exchange of water across the Fram Strait but the increase in salinity in the GLIN Seas region leads to a slightly more saline Arctic in the MioGIS simulation (Figure 2).

As the AMOC strenghtens in MioGIS, sea surface temperatures in the GLIN Seas region is also higher (+1°C). This leads to decreased sea-ice formation in coastal Greenland and in the Labrador Sea in MioGIS compared to MioCTL (Figure S5 in Supporting Information S1). These results show that the cooling effect of the ice sheet does not extend beyond Greenland because it is hampered by other dynamical processes, such as, here, an increase in NADW formation transporting additional heat poleward via a positive temperature-advection feedback.

Our results are consistent with those of Davini et al. (2015), who observe a slowdown of AMOC by 12% in the absence of an ice sheet over Greenland (25% in our case) in a modern configuration. The difference in simulated slowdown of the AMOC is probably related to a combination of a different model, pCO_2 levels and geography—and, in particular, the configuration of the Fram Strait (Hossain et al., 2020).

3.3. Consequences of the Closure of the Eastern Tethys Seaway on Water Exchanges Between the Indian and Atlantic Oceans and the Mediterranean Sea

Opening the ETS at 120 m depth, on the other hand, results in negligible changes in terms of SST, surface salinity and mixed layer depth (Figure 2d) in the GLIN Seas and Arctic Oceans. The AMOC index is also similar to the one of MioCTL (Figure 4). We explain below the reasons why the AMOC appears insensitive to changes in Tethys Seaway, contrary to previous modeling results (Z. Zhang et al., 2011) and commonly-accepted hypothesis in the literature (Woodruff & Savin, 1989; Wright et al., 1992).

First, the closure of the ETS causes a restructuring of water exchanges between the Mediterranean Sea and the Atlantic and Indian Oceans. In MioCTL, water exchange is only possible between the Mediterranean Sea and the Atlantic Ocean through the Gibraltar Gateway. Surface water flow is directed from the Atlantic Ocean to the

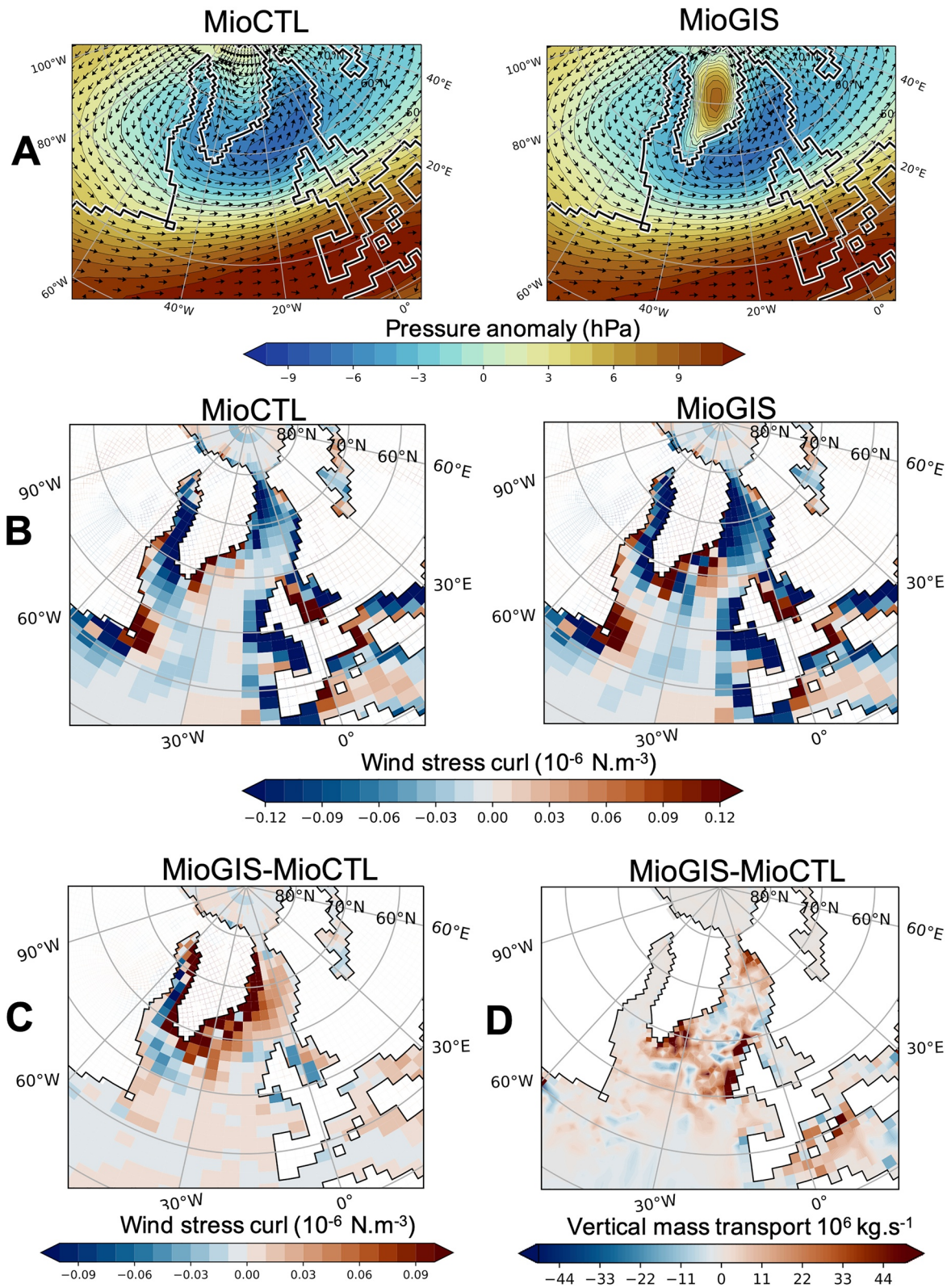

Figure 6. (a) In color, pressure anomaly (hPa), averaged over the winter, at ground level. The arrows indicate the average wind direction at 850 hPa. (b) Wind stress curl above the sea (10^{-6}N.m^{-3}) averaged over the year. (c) Differences in absolute value of Wind stress curl above the sea (10^{-6}N.m^{-3}) averaged over the year. (d) Differences in absolute value of vertical mass transport (10^{6} kg.s^{-1}) averaged over the year and the first 500 m depth. Values represent average on the last 100 years of each simulation.

Mediterranean Sea whereas subsurface flow is reversed (Figures S6 and S7 in Supporting Information S1). The difference between water flowing in and out of the Mediterranean Sea is smaller than 100 mSv (2.18 Sv in and 2.09 Sv out, compensated by runoff and P-E). In MioTet120, the majority of the water entering the Mediterranean Basin comes from the Indian Ocean (3.8 Sv) and then flows into the Atlantic Ocean (4.06 Sv). This net westward flow through the Mediterranean Sea is a remnant of the Circumglobal Tethys Current (de la Vara & Meijer, 2016). Most modeling studies describe an overall net flow in the ETS that is directed toward the Mediterranean Basin, with water transported from the Indian Ocean to the Atlantic Ocean through the Mediterranean Sea as seen in our simulations (Herold et al., 2011; Karami et al., 2011; von der Heydt & Dijkstra, 2006). In our simulations, there also exists a water flux that flows at depth from the Atlantic Ocean to the Mediterranean Sea which is consistent with the results of Karami et al. (2011).

Outflowing waters from the Mediterranean Sea are dragged into the North Atlantic Gyre along the North African coasts and then cross the Atlantic Ocean into the Caribbean Sea. Consequently, waters originating from the Indian Ocean return to the low latitudes in the Atlantic Ocean and hardly influence North Atlantic Ocean conditions, which explains the small difference between MioTet120 and MioCTL in the area of deep water formation in the North Atlantic. In addition, we note that there is almost no salinity gradient at the latitudes of the ETS between the Indian and the Atlantic Oceans, at least for shallow depths (Figure 7b), suggesting that there is no significant salt transport between these two oceans. The closure of the ETS also impacts water flow exchange between the Atlantic and Pacific Oceans across the Central American Seaway. In MioCTL, 6.21 Sv of waters is transported from the Atlantic to the Pacific and 13.84 Sv from the Pacific Ocean to the Atlantic Ocean. In MioTet120, more water is transported to the Pacific Ocean (+1.33 Sv) and less to the Atlantic Ocean (−2.51 Sv). This indicates that the extra water entering the Atlantic from the Mediterranean Sea when the ETS is open is mainly discharged to the Pacific Ocean through the Central American Seaway (consistent with Herold et al. (2011)).

Many studies suggest that the ETS was shallow or even intermittently closed as early as 22 Ma (Bialik et al., 2019; Harzhauser et al., 2007, 2009; Rögl, 1999; Sun et al., 2021). Our results are consistent with those of Hamon et al. (2013) in suggesting that the final closure of the ETS in the Miocene did not generate major changes in the AMOC, although the details of our and Hamon et al. (2013) simulations differ, in particular the depth of the ETS and Gibraltar Gateway. In particular, even though the ETS is shallower in our simulation than in Hamon et al. (2013), the flux through Gibraltar toward the Atlantic Ocean is higher (4 vs. 2.8 Sv in Hamon et al. (2013)) because the Gibraltar gateway is deeper in our paleogeography (1,350 m vs. 400 m in Hamon et al. (2013)). We note incidentally that changes in the Gibraltar gateway configuration have been suggested to impact the AMOC later in the Miocene (Capella et al., 2019; Flecker et al., 2015; Ivanovic et al., 2013; Ng et al., 2021). In contrast, the modeling study of Z. Zhang et al. (2011) suggests that the Tethys seaway closure was key to the evolution of NADW. In their simulations however both the Tethys Seaway and Central American Seaway have been closed simultaneously, which makes it difficult to decouple the relative impact of each seaway on their simulated NADW amplification. We note that a significant number of studies have shown that a primary effect of closing the Central American Seaway is to amplify NADW (Nisancioglu et al., 2003; Schneider & Schmittner, 2006; Sepulchre et al., 2014) and we speculate that it may well be the key driver of NADW increase in the results of Z. Zhang et al. (2011). In addition, Z. Zhang et al. (2011) use an Early Eocene paleogeography that is quite different from the Early Miocene and thus could also partly explain the contradictory results with our simulations.

Although the closure of the ETS has no impact on surface salinity of the North Atlantic, there is a significant salinity anomaly in Paratethyan waters (Figure 2c). In MioTet120, the Paratethys is considerably less salty than in MioCTL (−5 psu). When the ETS is closed, the salinity is relatively homogeneous between the Mediterranean Sea and the Paratethys (Figures 7a and 7b). There is a 6 mSv freshwater inflow (precipitation − evaporation + runoff) in the Paratethys in the MioTet120 simulation whereas it is restricted to −1 mSv in the MioCTL simulation. This difference in freshwater inflow is explained by higher precipitation over the Paratethys and its catchments (Figure 7c) with the ETS open. This additional water inflow in the MioTet120 simulation comes from a more humid atmosphere. By closing the ETS, a water surface is removed and replaced by a land surface causing a large negative evaporation anomaly at the seaway location (Figure 7d). The difference in salinity in the Paratethys basin between the two simulations can also be explained by a different oceanic circulation at the Mediterranean-Paratethys interface. In MioCTL, 0.453 Sv of water flow from the Paratethys to the Mediterranean Sea and 0.452 Sv flow in the opposite direction. In MioTet120, the flows into and out of the Paratethys are reduced to 0.391 and 0.397 Sv respectively (Figure S7 in Supporting Information S1). There is therefore more

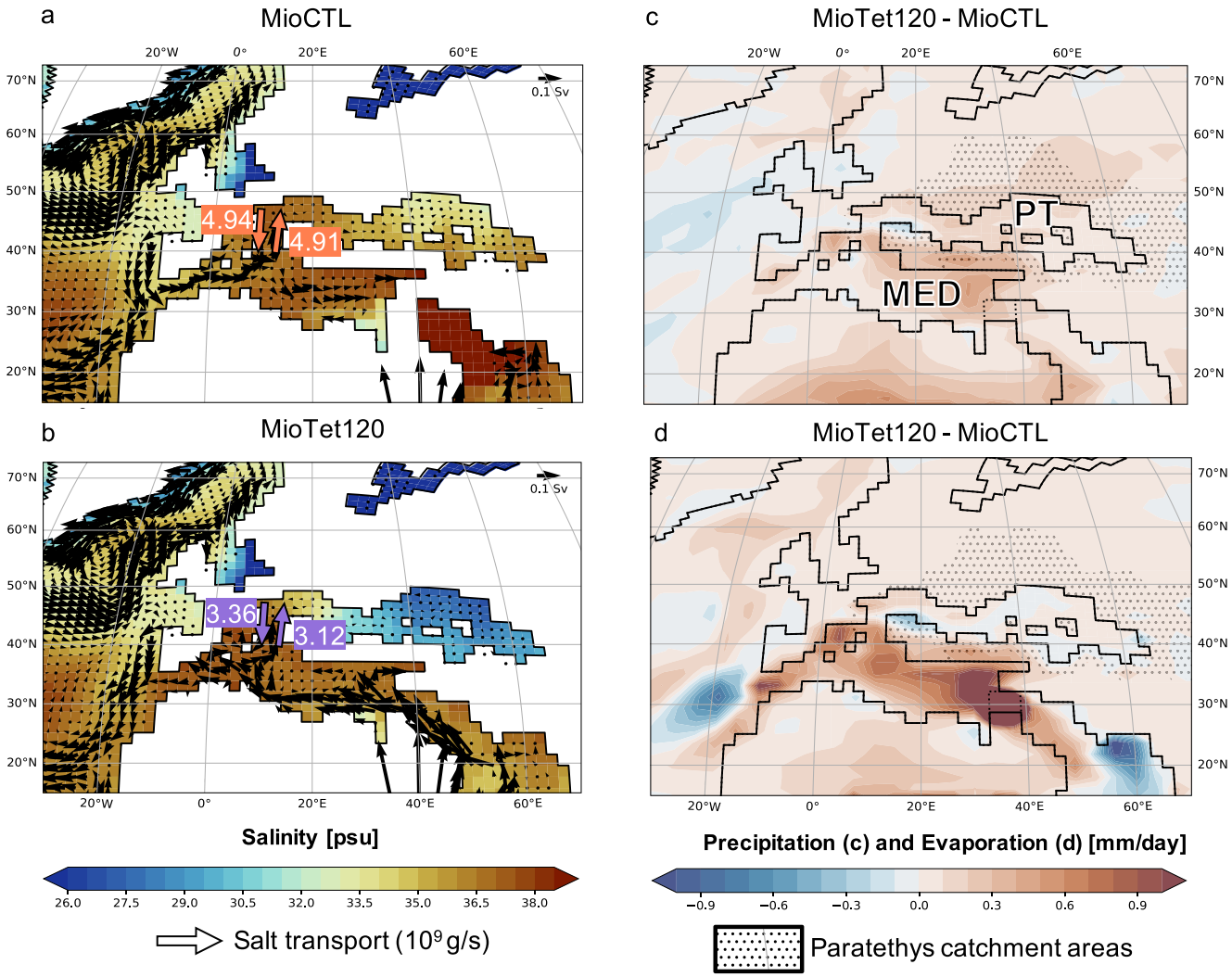

Figure 7. Left: Salinity (psu) for the first 100 m averaged over the year. The arrows indicate the direction of the flows and the streamflow in Sv (averaged over the year) (a) MioCTL and (b) MioTet120). The colored arrows indicate the salt transport budget (10^9 g/s). Right, (c) Differences in precipitation in mm/day averaged over the year (MioTet120-MioCTL). Right, (d) Differences in evaporation in mm/day averaged over the year (MioTet120-MioCTL). The dotted areas represent the catchment's areas draining into the Paratethys. Values represent average on the last 100 years of each simulation. MED: Mediterranean Sea. PT: Paratethys.

exchange between the Mediterranean Sea and the Paratethys when the ETS is closed with a larger input of salt as well (Figure 7). This is consistent with results from a box-model (Karami, 2011) which infers that the increase in exchange between seas is related to the modulation of flows between Atlantic, Mediterranean, Paratethys and Indian basins but cannot integrate the regional geographic complexity as in our simulations. The flow and exchange variations are due to the different structure of ocean currents in the Mediterranean Sea with an open or close Tethys Seaway. Indeed, the circulation is mainly east-west when the seaway is open, thereby limiting meridional exchanges with the Paratethys. As a concluding remark, we propose that both processes (hydrological cycle and oceanic advection of salt) lead to the increase in salinity of the Paratethys seen when closing the ETS.

4. Conclusion

Our simulations show that in the early Miocene, NADW formation was less intense—thus the AMOC was weaker—compared to the pre-industrial. This is a result of Miocene paleogeography (different configurations of some seaways), and perhaps also to a lesser extent by higher Miocene atmospheric pCO_2 conditions. The increased elevation induced by Greenland glaciation increases the wind stress curl over the Greenland and Nordic Seas. This increase favors vertical exchange through Ekman pumping, with deeper and more saline waters inducing

a positive salt-advection feedback that brings more salt from the North Atlantic to the Greenland, Labrador, Iceland and Nordic Seas. This increase in surface water salinity in the northern North Atlantic Ocean amplifies NADW formation. In the Miocene, possible episodes of Greenland glaciation may have favored and amplified NADW formation. In a context of present-day GIS melting, several studies suggest that the inflow of fresh water into the northern part of the North Atlantic Ocean may weaken the AMOC (Böning et al., 2016; Driesschaert et al., 2007). Our results suggest that it might also be relevant to take into account the effects of changing ice-sheet elevation and albedo induced by melting, as these induce changes in atmosphere circulation that slow down the AMOC. In contrast, the closure of the Eastern Tethys Seaway that occurred during the Miocene does not have a significant impact on the intensity of NADW formation.

Data Availability Statement

LMDZ, XIOS, NEMO and ORCHIDEE are released under the terms of the CeCILL license. OASIS-MCT is released under the terms of the Lesser GNU General Public License (LGPL). IPSL-CM5A2 source code is publicly available through (Pillot, 2022b). The mod.def file provides information regarding the different revisions used, namely:

- NEMOGCM branch nemo_v3_6_STABLE revision 6665
- XIOS2 branchs/xios-2.5 revision 1763
- IOIPSL/src svn tags/v2_2_2
- LMDZ5 branches/IPSLCM5A2.1 rev 3591
- branches/publications/ORCHIDEE IPSLCM5A2.1.r5307 rev 6336
- OASIS3-MCT 2.0 branch (rev 4775 IPSL server)

We recommend that you refer to the project website: http://forge.ipsl.jussieu.fr/igcmgdoc/wiki/Doc/Config/IPSLCM5A2 for a proper installation and compilation of the environment. All model outputs used in this study are available at Pillot (2022a).

Acknowledgments
We are grateful to the associate editor A. Farnsworth and the two anonymous reviewers for their relevant comments and suggestions that clearly improved the manuscript. We thank the CEA/CCRT for providing access to the HPC resources of TGCC under the allocation 2019-A0050102212 and 2020-A0090102212 made by GENCI and French ANR projects AMOR (YD, ANR-16-CE31-0020) and MioCarb (BSM, ANR-20-CE49-0002) for providing funding for this work. Colored figures in this paper were made with perceptually uniform, color-vision-deficiency-friendly scientific color maps, developed and distributed by F. Crameri (www.fabiocrameri.ch/colourmaps) (Crameri et al., 2020).

References

Allen, M. B., & Armstrong, H. A. (2008). Arabia–Eurasia collision and the forcing of mid-Cenozoic global cooling. *Palaeogeography, Palaeoclimatology, Palaeoecology*, *265*(1–2), 52–58. https://doi.org/10.1016/j.palaeo.2008.04.021

Aumont, O., Ethé, C., Tagliabue, A., Bopp, L., & Gehlen, M. (2015). PISCES-v2: An ocean biogeochemical model for carbon and ecosystem studies. *Geoscientific Model Development*, *8*(8), 2465–2513. https://doi.org/10.5194/gmd-8-2465-2015

Baatsen, M., von der Heydt, A. S., Huber, M., Kliphuis, M. A., Bijl, P. K., Sluijs, A., & Dijkstra, H. A. (2020). The middle to late Eocene greenhouse climate modelled using the CESM 1.0.5. *Climate of the Past*, *16*(6), 2573–2597. https://doi.org/10.5194/cp-16-2573-2020

Bernard, T., Steer, P., Gallagher, K., Szulc, A., Whitham, A., & Johnson, C. (2016). Evidence for Eocene–Oligocene glaciation in the landscape of the East Greenland margin. *Geology*, *44*(11), 895–898. https://doi.org/10.1130/G38248.1

Bialik, O. M., Frank, M., Betzler, C., Zammit, R., & Waldmann, N. D. (2019). Two-step closure of the Miocene Indian Ocean gateway to the Mediterranean. *Scientific Reports*, *9*(1), 8842. https://doi.org/10.1038/s41598-019-45308-7

Bierman, P. R., Shakun, J. D., Corbett, L. B., Zimmerman, S. R., & Rood, D. H. (2016). A persistent and dynamic East Greenland Ice Sheet over the past 7.5 million years. *Nature*, *540*(7632), 256–260. https://doi.org/10.1038/nature20147

Böning, C. W., Behrens, E., Biastoch, A., Getzlaff, K., & Bamber, J. L. (2016). Emerging impact of Greenland meltwater on deepwater formation in the North Atlantic Ocean. *Nature Geoscience*, *9*(7), 523–527. https://doi.org/10.1038/ngeo2740

Borrelli, C., Cramer, B. S., & Katz, M. E. (2014). Bipolar Atlantic deepwater circulation in the middle-late Eocene: Effects of Southern Ocean gateway openings. *Paleoceanography*, *29*(4), 308–327. https://doi.org/10.1002/2012PA002444

Brierley, C. M., & Fedorov, A. V. (2016). Comparing the impacts of Miocene–Pliocene changes in inter-ocean gateways on climate: Central American Seaway, Bering Strait, and Indonesia. *Earth and Planetary Science Letters*, *444*, 116–130. https://doi.org/10.1016/j.epsl.2016.03.010

Burls, N. J., Bradshaw, C., De Boer, A. M., Herold, N., Huber, M., Pound, M., et al. (2021). Simulating Miocene warmth: Insights from an opportunistic multi-model ensemble (MioMIP1). *Paleoceanography and Paleoclimatology*, *36*, e2020PA004054. https://doi.org/10.1029/2020PA004054

Burls, N. J., & Fedorov, A. V. (2017). Wetter subtropics in a warmer world: Contrasting past and future hydrological cycles. *Proceedings of the National Academy of Sciences of the United States of America*, *114*(49), 12888–12893. https://doi.org/10.1073/pnas.1703421114

Butt, F. A., ElverhØi, A., Forsberg, C. F., & Solheim, A. (2001). Evolution of the Scoresby Sund fan, central East Greenland - evidence from ODP site987. *Norsk Geologisk Tidsskrift*, *81*, 3–15.

Capella, W., Flecker, R., Hernández-Molina, F. J., Simon, D., Meijer, P. T., Rogerson, M., et al. (2019). Mediterranean isolation preconditioning the Earth System for late Miocene climate cooling. *Scientific Reports*, *9*(1), 3795. https://doi.org/10.1038/s41598-019-40208-2

Coxall, H. K., Huck, C. E., Huber, M., Lear, C. H., Legarda-Lisarri, A., O'Regan, M., et al. (2018). Export of nutrient rich Northern Component Water preceded early Oligocene Antarctic glaciation. *Nature Geoscience*, *11*(3), 190–196. https://doi.org/10.1038/s41561-018-0069-9

Crameri, F., Shephard, G. E., & Heron, P. J. (2020). The misuse of colour in science communication. *Nature Communications*, *11*(1), 5444. https://doi.org/10.1038/s41467-020-19160-7

Davies, R., Cartwright, J., Pike, J., & Line, C. (2001). Early Oligocene initiation of North Atlantic deep water formation. *Nature*, *410*(6831), 917–920. https://doi.org/10.1038/35073551

Davini, P., von Hardenberg, J., Filippi, L., & Provenzale, A. (2015). Impact of Greenland orography on the Atlantic Meridional overturning circulation. *Geophysical Research Letters*, *42*(3), 871–879. https://doi.org/10.1002/2014GL062668

DeConto, R. M., Pollard, D., Wilson, P. A., Pälike, H., Lear, C. H., & Pagani, M. (2008). Thresholds for Cenozoic bipolar glaciation. *Nature*, *455*(7213), 652–656. https://doi.org/10.1038/nature07337

de la Vara, A., & Meijer, P. (2016). Response of Mediterranean circulation to Miocene shoaling and closure of the Indian gateway: A model study. *Palaeogeography, Palaeoclimatology, Palaeoecology*, *442*, 96–109. https://doi.org/10.1016/j.palaeo.2015.11.002

Driesschaert, E., Fichefet, T., Goosse, H., Huybrechts, P., Janssens, I., Mouchet, A., et al. (2007). Modeling the influence of Greenland Ice Sheet melting on the Atlantic meridional overturning circulation during the next millennia. *Geophysical Research Letters*, *34*(10), L10707. https://doi.org/10.1029/2007GL029516

Dufresne, J.-L., Foujols, M.-A., Denvil, S., Caubel, A., Marti, O., Aumont, O., et al. (2013). Climate change projections using the IPSL-CM5 Earth System Model: From CMIP3 to CMIP5. *Climate Dynamics*, *40*(9–10), 2123–2165. https://doi.org/10.1007/s00382-012-1636-1

Ehlers, B.-M., & Jokat, W. (2013). Paleo-bathymetry of the northern North Atlantic and consequences for the opening of the Fram Strait. *Marine Geophysical Researches*, *34*(1), 25–43. https://doi.org/10.1007/s11001-013-9165-9

Eldrett, J. S., Harding, I. C., Wilson, P. A., Butler, E., & Roberts, A. P. (2007). Continental ice in Greenland during the Eocene and Oligocene. *Nature*, *446*(7132), 176–179. https://doi.org/10.1038/nature05591

Ferreira, D., Cessi, P., Coxall, H. K., de Boer, A., Dijkstra, H. A., Drijfhout, S. S., et al. (2018). Atlantic-Pacific Asymmetry in deep water formation. *Annual Review of Earth and Planetary Sciences*, *46*(1), 327–352. https://doi.org/10.1146/annurev-earth-082517-010045

Fichefet, T., & Maqueda, M. A. M. (1997). Sensitivity of a global sea ice model to the treatment of ice thermodynamics and dynamics. *Journal of Geophysical Research*, *102*(C6), 12609–12646. https://doi.org/10.1029/97JC00480

Flecker, R., Krijgsman, W., Capella, W., de Castro Martíns, C., Dmitrieva, E., Mayser, J. P., et al. (2015). Evolution of the Late Miocene Mediterranean–Atlantic gateways and their impact on regional and global environmental change. *Earth-Science Reviews*, *150*, 365–392. https://doi.org/10.1016/j.earscirev.2015.08.007

Gladenkov, A. Y., & Gladenkov, Y. B. (2004). Onset of connections between the Pacific and Arctic Oceans through the Bering Strait in the Neogene. *Stratigraphy and Geological Correlation*, *12*(2), 13.

Goldner, A., Herold, N., & Huber, M. (2014). The challenge of simulating the warmth of the mid-Miocene climatic optimum in CESM1. *Climate of the Past*, *10*(2), 523–536. https://doi.org/10.5194/cp-10-523-2014

Hamon, N., Sepulchre, P., Lefebvre, V., & Ramstein, G. (2013). The role of Eastern Tethys Seaway closure in the middle Miocene climatic transition (ca. 14 Ma). *Climate of the Past*, *9*(6), 2687–2702. https://doi.org/10.5194/cp-9-2687-2013

Harzhauser, M., Kroh, A., Mandic, O., Piller, W. E., Göhlich, U., Reuter, M., & Berning, B. (2007). Biogeographic responses to geodynamics: A key study all around the Oligo–Miocene Tethyan Seaway. *Zoologischer Anzeiger*, *246*(4), 241–256. https://doi.org/10.1016/j.jcz.2007.05.001

Harzhauser, M., Reuter, M., Piller, W. E., Berning, B., Kroh, A., & Mandic, O. (2009). Oligocene and early Miocene gastropods from Kutch (NW India) document an early biogeographic switch from Western Tethys to Indo-Pacific. *Paläontologische Zeitschrift*, *83*(3), 333–372. https://doi.org/10.1007/s12542-009-0025-5

Helland, P., & Holmes, M. (1997). Surface textural analysis of quartz sand grains from ODP Site 918 off the southeast coast of Greenland suggests glaciation of southern Greenland at 11 Ma. *Palaeogeography, Palaeoclimatology, Palaeoecology*, *135*(1–4), 109–121. https://doi.org/10.1016/S0031-0182(97)00025-4

Herold, N., Huber, M., & Müller, R. D. (2011). Modeling the Miocene climatic optimum. Part I: Land and atmosphere. *Journal of Climate*, *24*(24), 6353–6372. https://doi.org/10.1175/2011JCLI4035.1

Hossain, A., Knorr, G., Lohmann, G., Stärz, M., & Jokat, W. (2020). Simulated thermohaline fingerprints in response to different Greenland-Scotland Ridge and Fram Strait subsidence histories. *Paleoceanography and Paleoclimatology*, *35*(7), e2019PA003842. https://doi.org/10.1029/2019PA003842

Hourdin, F., Foujols, M.-A., Codron, F., Guemas, V., Dufresne, J.-L., Bony, S., et al. (2013). Impact of the LMDZ atmospheric grid configuration on the climate and sensitivity of the IPSL-CM5A coupled model. *Climate Dynamics*, *40*(9–10), 2167–2192. https://doi.org/10.1007/s00382-012-1411-3

Hu, A., Meehl, G. A., Han, W., Otto-Bliestner, B., Abe-Ouchi, A., & Rosenbloom, N. (2015). Effects of the Bering Strait closure on AMOC and global climate under different background climates. *Progress in Oceanography*, *132*, 174–196. https://doi.org/10.1016/j.pocean.2014.02.004

Hüsing, S. K., Zachariasse, W.-J., van Hinsbergen, D. J. J., Krijgsman, W., Inceöz, M., Harzhauser, M., et al. (2009). Oligocene–Miocene basin evolution in SE Anatolia, Turkey: Constraints on the closure of the eastern Tethys gateway. *Geological Society, London, Special Publications*, *311*(1), 107–132. https://doi.org/10.1144/SP311.4

Hutchinson, D. K., Coxall, H. K., ORegan, M., Nilsson, J., Caballero, R., & de Boer, A. M. (2019). Arctic closure as a trigger for Atlantic overturning at the Eocene-Oligocene transition. *Nature Communications*, *10*(1), 3797. https://doi.org/10.1038/s41467-019-11828-z

Hutchinson, D. K., de Boer, A. M., Coxall, H. K., Caballero, R., Nilsson, J., & Baatsen, M. (2018). Climate sensitivity and meridional overturning circulation in the late Eocene using GFDL CM2.1. *Climate of the Past*, *14*(6), 789–810. https://doi.org/10.5194/cp-14-789-2018

Ivanovic, R. F., Valdes, P. J., Flecker, R., Gregoire, L. J., & Gutjahr, M. (2013). The parameterisation of Mediterranean–Atlantic water exchange in the Hadley Centre model HadCM3, and its effect on modelled North Atlantic climate. *Ocean Modelling*, *62*, 11–16. https://doi.org/10.1016/j.ocemod.2012.11.002

Jakobsson, M., Backman, J., Rudels, B., Nycander, J., Frank, M., Mayer, L., et al. (2007). The early Miocene onset of a ventilated circulation regime in the Arctic Ocean. *Nature*, *447*(7147), 986–990. https://doi.org/10.1038/nature05924

John, K. E. K. S., & Krissek, L. A. (2002). The late Miocene to Pleistocene ice-rafting history of southeast Greenland. *Boreas*, *31*, 28–35. https://doi.org/10.1111/j.1502-3885.2002.tb01053.x

Karami, M. P., de Leeuw, A., Krijgsman, W., Meijer, P., & Wortel, M. (2011). The role of gateways in the evolution of temperature and salinity of semi-enclosed basins: An oceanic box model for the Miocene Mediterranean Sea and Paratethys. *Global and Planetary Change*, *17*(1–2), 73–88. https://doi.org/10.1016/j.gloplacha.2011.07.011

Katz, M. E., Cramer, B. S., Toggweiler, J. R., Esmay, G., Liu, C., Miller, K. G., et al. (2011). Impact of Antarctic circumpolar current development on late Paleogene Ocean structure. *Science*, *332*(6033), 1076–1079. https://doi.org/10.1126/science.1202122

Knutz, P. C., Hopper, J. R., Gregersen, U., Nielsen, T., & Japsen, P. (2015). A contourite drift system on the Baffin Bay–West Greenland margin linking Pliocene Arctic warming to poleward ocean circulation. *Geology*, *43*(10), 907–910. https://doi.org/10.1130/G36927.1

Krapp, M., & Jungclaus, J. H. (2011). The Middle Miocene climate as modelled in an atmosphere-ocean-biosphere model. *Climate of the Past*, *7*(4), 1169–1188. https://doi.org/10.5194/cp-7-1169-2011

Krinner, G., Viovy, N., de Noblet-Ducoudré, N., Ogée, J., Polcher, J., Friedlingstein, P., et al. (2005). A dynamic global vegetation model for studies of the coupled atmosphere-biosphere system: DVGM for coupled climate studies. *Global Biogeochemical Cycles*, *19*(1), GB1015. https://doi.org/10.1029/2003GB002199

Lagabrielle, Y., Goddéris, Y., Donnadieu, Y., Malavieille, J., & Suarez, M. (2009). The tectonic history of Drake Passage and its possible impacts on global climate. *Earth and Planetary Science Letters*, *279*(3–4), 197–211. https://doi.org/10.1016/j.epsl.2008.12.037

Langton, S. J., Rabideaux, N. M., Borrelli, C., & Katz, M. E. (2016). Southeastern Atlantic deep-water evolution during the late-middle Eocene to earliest Oligocene (Ocean drilling Program site 1263 and deep sea drilling Project site 366). *Geosphere*, *12*(3), 1032–1047. https://doi.org/10.1130/GES01268.1

Lunt, D. J., Bragg, F., Chan, W.-L., Hutchinson, D. K., Ladant, J.-B., Morozova, P., et al. (2021). DeepMIP: Model intercomparison of early Eocene climatic optimum (EECO) large-scale climate features and comparison with proxy data. *Climate of the Past*, *17*(1), 203–227. https://doi.org/10.5194/cp-17-203-2021

Lunt, D. J., de Noblet-Ducoudré, N., & Charbit, S. (2004). Effects of a melted Greenland Ice Sheet on climate, vegetation, and the cryosphere. *Climate Dynamics*, *23*(7–8), 679–694. https://doi.org/10.1007/s00382-004-0463-4

Lunt, D. J., Foster, G. L., Haywood, A. M., & Stone, E. J. (2008). Late Pliocene Greenland glaciation controlled by a decline in atmospheric CO_2 levels. *Nature*, *454*(7208), 1102–1105. https://doi.org/10.1038/nature07223

Madec, G., & Team, N. S. (2015). Nemo ocean engine (Vol. *27*, p. 396). https://doi.org/10.5281/zenodo.1464816

Montes, C., Cardona, A., Jaramillo, C., Pardo, A., Silva, J. C., Valencia, V., et al. (2015). Middle Miocene closure of the central American Seaway. *Science*, *348*(6231), 226–229. https://doi.org/10.1126/science.aaa2815

Ng, Z. L., Hernández-Molina, F. J., Duarte, D., Sierro, F. J., Ledesma, S., Rogerson, M., et al. (2021). Latest Miocene restriction of the Mediterranean outflow water: A perspective from the Gulf of Cádiz. *Geo-Marine Letters*, *41*(2), 23. https://doi.org/10.1007/s00367-021-00693-9

Nisancioglu, K. H., Raymo, M. E., & Stone, P. H. (2003). Reorganization of Miocene deep water circulation in response to the shoaling of the central American Seaway: Reorganization of Miocene deep water circulation. *Paleoceanography*, *18*(1), 1006. https://doi.org/10.1029/2002PA000767

Okay, A. I., Zattin, M., & Cavazza, W. (2010). Apatite fission-track data for the Miocene Arabia-Eurasia collision. *Geology*, *38*(1), 35–38. https://doi.org/10.1130/G30234.1

Pierce, E. L., van de Flierdt, T., Williams, T., Hemming, S. R., Cook, C. P., & Passchier, S. (2017). Evidence for a dynamic East Antarctic ice sheet during the mid-Miocene climate transition. *Earth and Planetary Science Letters*, *478*, 1–13. https://doi.org/10.1016/j.epsl.2017.08.011

Pillot, Q. (2022a). Evolution of ocean circulation in the north Atlantic Ocean during the Miocene: Impact of the Greenland Ice Sheet and the Eastern Tethys Seaway [Dataset]. Zenodo. https://doi.org/10.5281/zenodo.6671070

Pillot, Q. (2022b). IPSL-CM5A2 source code used for "Evolution of ocean circulation in the north Atlantic Ocean during the Miocene: Impact of the Greenland Ice Sheet and the Eastern Tethys Seaway" [Software]. Zenodo. https://doi.org/10.5281/zenodo.6772699

Poblete, F., Dupont-Nivet, G., Licht, A., van Hinsbergen, D., Roperch, P., Mihalynuk, M., et al. (2021). Towards interactive global paleogeographic maps, new reconstructions at 60, 40 and 20 Ma. *Earth-Science Reviews*, *214*, 103508. https://doi.org/10.1016/j.earscirev.2021.103508

Poore, H. R., Samworth, R., White, N. J., Jones, S. M., & McCave, I. N. (2006). Neogene overflow of northern component water at the Greenland-Scotland Ridge: Neogene overflow of NCW. *Geochemistry Geophysics Geosystems*, *7*(6), Q06010. https://doi.org/10.1029/2005GC001085

Rae, J. W., Zhang, Y. G., Liu, X., Foster, G. L., Stoll, H. M., & Whiteford, R. D. (2021). Atmospheric CO_2 over the past 66 million years from marine archives. *Annual Review of Earth and Planetary Sciences*, *49*(1), 609–641. https://doi.org/10.1146/annurev-earth-082420-063026

Reuter, M., Piller, W. E., Harzhauser, M., Mandic, O., Berning, B., Rögl, F., et al. (2009). The oligo-/Miocene Qom formation (Iran): Evidence for an early Burdigalian restriction of the Tethyan Seaway and closure of its Iranian gateways. *International Journal of Earth Sciences*, *98*(3), 627–650. https://doi.org/10.1007/s00531-007-0269-9

Rögl, F. (1999). Mediterranean and paratethys. Facts and hypotheses of an Oligocene to Miocene paleogeography (short overview). *Geologica Carpathica*, *11*. http://www.geologicacarpathica.com/browse-journal/volumes/50-4/article-138/

Scher, H. D., & Martin, E. E. (2008). Oligocene deep water export from the north Atlantic and the development of the Antarctic circumpolar current examined with neodymium isotopes: Oligocene thermohaline transition. *Paleoceanography*, *23*(1), PA1205. https://doi.org/10.1029/2006PA001400

Schneider, B., & Schmittner, A. (2006). Simulating the impact of the Panamanian seaway closure on ocean circulation, marine productivity and nutrient cycling. *Earth and Planetary Science Letters*, *246*(3–4), 367–380. https://doi.org/10.1016/j.epsl.2006.04.028

Sepulchre, P., Arsouze, T., Donnadieu, Y., Dutay, J.-C., Jaramillo, C., Le Bras, J., et al. (2014). Consequences of shoaling of the Central American Seaway determined from modeling Nd isotopes. *Paleoceanography*, *29*(3), 176–189. https://doi.org/10.1002/2013PA002501

Sepulchre, P., Caubel, A., Ladant, J.-B., Bopp, L., Boucher, O., Braconnot, P., et al. (2020). IPSL-CM5A2—An Earth system model designed for multi-millennial climate simulations. *Geoscientific Model Development*, *13*(7), 3011–3053. https://doi.org/10.5194/gmd-13-3011-2020

Sosdian, S. M., Greenop, R., Hain, M. P., Foster, G. L., Pearson, P. N., & Lear, C. H. (2018). Constraining the evolution of Neogene ocean carbonate chemistry using the boron isotope pH proxy. *Earth and Planetary Science Letters*, *498*, 362–376. https://doi.org/10.1016/j.epsl.2018.06.017

Stärz, M., Jokat, W., Knorr, G., & Lohmann, G. (2017). Threshold in North Atlantic-Arctic Ocean circulation controlled by the subsidence of the Greenland-Scotland Ridge. *Nature Communications*, *8*(1), 15681. https://doi.org/10.1038/ncomms15681

Sun, J., Sheykh, M., Ahmadi, N., Cao, M., Zhang, Z., Tian, S., et al. (2021). Permanent closure of the Tethyan Seaway in the northwestern Iranian Plateau driven by cyclic sea-level fluctuations in the late Middle Miocene. *Palaeogeography, Palaeoclimatology, Palaeoecology*, *564*, 110172. https://doi.org/10.1016/j.palaeo.2020.110172

Talley, L. (2013). Closure of the global overturning circulation through the Indian, Pacific, and Southern Oceans: Schematics and transports. *Oceanography*, *26*(1), 80–97. https://doi.org/10.5670/oceanog.2013.07

Tan, N., Ladant, J.-B., Ramstein, G., Dumas, C., Bachem, P., & Jansen, E. (2018). Dynamic Greenland ice sheet driven by pCO_2 variations across the Pliocene Pleistocene transition. *Nature Communications*, *9*(1), 4755. https://doi.org/10.1038/s41467-018-07206-w

Toniazzo, T., Gregory, J. M., & Huybrechts, P. (2004). Climatic impact of a Greenland deglaciation and its possible irreversibility. *Journal of Climate*, *17*(1), 13–33. https://doi.org/10.1175/1520-0442(2004)017<0021:cioagd>2.0.co;2

Toumoulin, A., Donnadieu, Y., Ladant, J.-B., Batenburg, S. J., Poblete, F., & Dupont-Nivet, G. (2020). Quantifying the effect of the Drake Passage opening on the Eocene Ocean. *Paleoceanography and Paleoclimatology*, *35*(8), e2020PA003889. https://doi.org/10.1029/2020PA003889

Tripati, A. K., Eagle, R. A., Morton, A., Dowdeswell, J. A., Atkinson, K. L., Bahé, Y., et al. (2008). Evidence for glaciation in the northern hemisphere back to 44 Ma from ice-rafted debris in the Greenland Sea. *Earth and Planetary Science Letters*, *265*(1–2), 112–122. https://doi.org/10.1016/j.epsl.2007.09.045

Valcke, S. (2013). The OASIS3 coupler: A European climate modelling community software. *Geoscientific Model Development*, *6*(2), 373–388. https://doi.org/10.5194/gmd-6-373-2013

Via, R. K., & Thomas, D. J. (2006). Evolution of Atlantic thermohaline circulation: Early Oligocene onset of deep-water production in the north Atlantic. *Geology*, *34*(6), 441. https://doi.org/10.1130/G22545.1

von der Heydt, A., & Dijkstra, H. A. (2006). Effect of ocean gateways on the Global ocean circulation in the late Oligocene and early Miocene: Oligocene/Miocene ocean circulation. *Paleoceanography*, *21*(1). https://doi.org/10.1029/2005PA001149

Woodruff, F., & Savin, S. M. (1989). Miocene deepwater oceanography. *Paleoceanography*, *4*(1), 87–140. https://doi.org/10.1029/PA004i001p00087

Wright, J. D., & Miller, K. G. (1993). Southern Ocean influences on late Eocene to Miocene deepwater circulation. In J. P. Kennett & D. A. Warnke (Eds.), *Antarctic Research Series* (Vol. 60, pp. 1–25). American Geophysical Union. https://doi.org/10.1029/AR060p0001

Wright, J. D., Miller, K. G., & Fairbanks, R. G. (1992). Early and middle Miocene stable isotopes: Implications for deepwater circulation and climate. *Paleoceanography*, *7*(3), 357–389. https://doi.org/10.1029/92PA00760

Zhang, Y., Huck, T., Lique, C., Donnadieu, Y., Ladant, J.-B., Rabineau, M., & Aslanian, D. (2020). Early Eocene vigorous ocean overturning and its contribution to a warm Southern Ocean. *Climate of the Past*, *16*(4), 1263–1283. https://doi.org/10.5194/cp-16-1263-2020

Zhang, Z., Nisancioglu, K. H., Flatøy, F., Bentsen, M., Bethke, I., & Wang, H. (2011). Tropical seaways played a more important role than high latitude seaways in Cenozoic cooling. *Climate of the Past*, *7*(3), 801–813. https://doi.org/10.5194/cp-7-801-2011